Materials Research Bulletin 47 (2012) 1568–1571

Contents lists available at SciVerse ScienceDirect

Materials Research Bulletin

journal homepage: www.elsevier.com/locate/matresbu

Physical properties of amorphous Mo-doped In–Ga–Zn–O films grown by magnetron co-sputtering technique

Shiu-Jen Liu [a,*], Hau-Wei Fang [b], Jang-Hsing Hsieh [c], Jenh-Yih Juang [d]

[a] Department of Mathematics and Science (Precollege), National Taiwan Normal University, Linkou Dist., New Taipei City 24449, Taiwan
[b] Department of Materials Science and Engineering, National Chiao Tung University, Hsinchu 30010, Taiwan
[c] Department of Materials Engineering, Mingchi University of Technology, Taishan Dist., New Taipei City 24301, Taiwan
[d] Department of Electrophysics, National Chiao Tung University, Hsinchu 30010, Taiwan

ARTICLE INFO

Article history:
Received 12 October 2011
Received in revised form 10 February 2012
Accepted 15 February 2012
Available online 24 February 2012

Keywords:
A. Amorphous materials
A. Semiconductors
B. Sputtering
D. Electrical properties
D. Magnetic properties
D. Optical properties

ABSTRACT

Amorphous thin films of In–Ga–Zn–O (a-IGZO) doped with Mo have been fabricated by using magnetron co-sputtering technique. The Mo concentration in a-IGZO films was modulated by varying the sputtering power applied on the Mo target. The electrical, optical and magnetic properties of Mo-doped a-IGZO films grown on glasses were investigated. The carrier density and mobility of a-IGZO films can be remarkably enhanced by low concentration Mo doping. On the other hand, the optical bandgap of a-IGZO films is not significantly affected by Mo doping. However, the transmission is decreased with increasing the Mo doping. Moreover, all Mo-doped films exhibit room-temperature ferromagnetism.

1. Introduction

Amorphous transparent conducting oxides (a-TCOs) are promising materials owing to their applications on optoelectronic devices such as thin film transistors (TFTs) used in flat panel displays [1,2]. One of the most attractive a-TCO is amorphous $InGaZnO_4$ (a-IGZO) which has been demonstrated to be able to work as the active layers in the high-performance TFTs fabricated on flexible substrates at room temperature [1] and used in large-size panels [3]. IGZO has a complex structure with alternating InO_2 and $GaZnO_2$ layers [4]. Due to the unique electronic structure in which the conduction paths of carriers in IGZO are composed of extended spherical s orbitals of heavy metal cations, the carrier transport is not affected by the chemical bond distortion and IGZO exhibits large electron mobility even in amorphous structure.

Many groups are devoted to the research and development of a-IGZO based TFTs in recent years. Theoretical calculation of electronic structure [4] and fundamental studies on optical and electrical properties of crystalline and amorphous IGZO films have also attracted much attention [5,6]. However, the physical properties of a-IGZO films doped with transition-metal impurities have rarely investigated [7,8]. In the meanwhile, the carrier mobility of In_2O_3 films has been reported to be drastically enhanced by Mo doping [9,10]. A theoretical model based on magnetic interactions was proposed to explain the enhancement of carrier mobility in Mo-doped In_2O_3 films [11]. The experimental and theoretical results of Mo-doped In_2O_3 urge us to explore the effects of Mo doping on physical properties of a-IGZO films. The enhancement of carrier mobility and room-temperature ferromagnetism induced by Mo doping were observed.

2. Experimental

The Mo-doped In–Ga–Zn–O films used in this study were prepared by using magnetron co-sputtering technique. The sputtering was conducted with a 75 W rf power applied on a $InGaZnO_4$ target and a various dc power ranging between 2 and 5 W applied on a metallic Mo target. Both targets were 2 in. in diameter and 99.99% in purity. Corning 1737 glasses were used as substrates and placed 45° to the targets surface with a substrate-to-target distance of 10 cm. During sputtering, the substrate temperature was kept at 150 °C and the flow rates of argon and oxygen were 17.5 and 10.5 sccm, respectively. The pressure of the chamber during sputtering was 1.2×10^{-2} Torr. After a 40-min sputtering, the films were cooled down to room temperature. The thickness of the sputtered films was determined to be about

* Corresponding author. Tel.: +886 2 77148405; fax: +886 2 26022617.
E-mail address: sjliu@ntnu.edu.tw (S.-J. Liu).

0025-5408/$ – see front matter © 2012 Elsevier Ltd. All rights reserved.
doi:10.1016/j.materresbull.2012.02.021

Table 1
The dc power (P) applied on the Mo target and Mo content ratios (x = [Mo]/[In] at.%) of thin-film samples used in this study. The sample #1 is the undoped In–Ga–Zn–O film.

	Sample no.				
	#1	#2	#3	#4	#5
P (W)	0	2	3	4	5
x (at.%)	0	3.8	7.6	9.9	18.1

100 nm by using a surface profilometer (Alpha Step 500, Tencor Instruments). The Mo content ratio [Mo]/[In] of the doped In–Ga–Zn–O films was measured by using energy dispersive X-ray spectroscopy and is denoted as x at.% (as listed in Table 1). The crystal structure of the films was examined by using X-ray diffraction (XRD) scans with Cu Kα radiation (PANalytical X'Pert PRO MPD). The electrical properties including resistivity, carrier concentration and carrier mobility were carried out using the four-probe van der Pauw method. The valence state of Mo ions was investigated by X-ray photoelectron spectroscopy (XPS) analysis using the Thermo VG Scientific ESCALAB 250 system with a Al Kα X-ray source (1486.6 eV). The analysis chamber is equipped with a flood gun used for charge compensation when necessary. The XPS spectra are referenced to the C 1s photoemission line of 284.8 eV. The optical measurements of the films were recorded using a UV–Vis double beam spectrometer (JASCO V570) in the wavelength of 200–900 nm. The room-temperature magnetization versus magnetic field $M(H)$ curves were performed on a Quantum Design superconducting quantum interference device magnetometer.

3. Results and discussion

The amorphous structure of all films was confirmed by the XRD scans shown in Fig. 1. There is no sharp peak observed in all XRD curves. The broad peaks located at around $2\theta = 22^\circ$ are contributed by the glass substrates.

XPS measurements were conducted on all samples to determine the valence state of Mo ions in the films. The measured Mo 3d spectra are shown in Fig. 2. At the first glance, there is no peak observed in the Mo 3d region for sample #1, the undoped a-IGZO film. Two peaks are observed for sample #2 and three peaks are observed for samples #3, #4 and #5. These peaks are labeled as G1, G2 and G3 according to their locations, i.e., binding energy. The exact values of binding energy of these Mo 3d peaks and possible contributions to these peaks are listed in Table 2. The G1 peaks are contributed by the Mo^{6+} $3d_{3/2}$ level [12]. The G2 peaks could be a combination of Mo^{6+} $3d_{5/2}$ and Mo^{4+} $3d_{3/2}$ peaks [13]. The G3 peaks

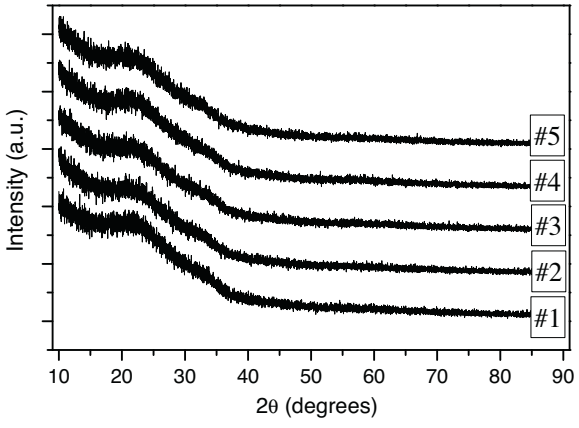

Fig. 1. XRD patterns of all films. The broad peaks located at about $2\theta = 22^\circ$ come from the glass substrates. The figures denote the sample number (listed in Table 1).

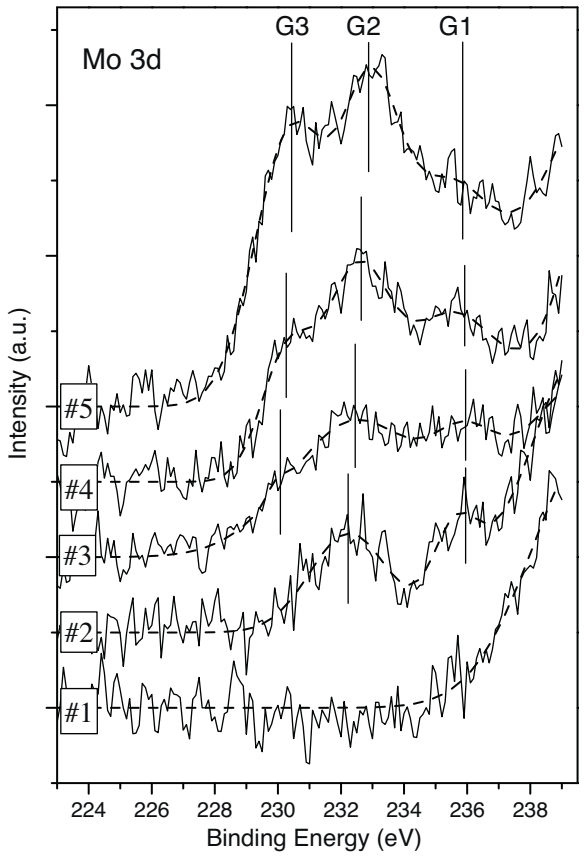

Fig. 2. XPS spectra in the Mo 3d region of the Mo-doped a-IGZO films. The smoothing lines (dash lines) are obtained by means of curve fitting using Gaussian functions and the backgrounds are not subtracted. G1, G2 and G3 denoted as the locations of Gaussian peaks which comprise the smoothing curves in the Mo 3d region.

are assigned to the Mo^{4+} $3d_{5/2}$ level. It can be deduced from the data listed in Table 2, the valence of Mo ions doped in sample #2 is 6+, and the valences of Mo ions doped in samples #3, #4 and #5 are 6+ and 4+. Moreover, since the binding energy of Mo^{4+} $3d_{3/2}$ is higher than that of Mo^{6+} $3d_{5/2}$, as shown in Table 2, the shift of the G2 peaks of samples #3, #4 and #5 toward higher energy indicates the increase of the $[Mo^{4+}]/[Mo^{6+}]$ content ratio with increasing the Mo doping concentration. The increase of $[Mo^{4+}]/[Mo^{6+}]$ content ratio can also be confirmed by the increase of the intensity of the G3 peaks with increasing the Mo concentration.

Fig. 3 displays the dependence of electrical properties including resistivity, carrier concentration, and mobility on the Mo content

Table 2
The binding energy of G1, G2 and G3 peaks observed in XPS curves as well as those of Mo^{4+} 3d and Mo^{6+} 3d levels adopted from Refs. [12,13].

Sample no.	G1 (eV)	G2 (eV)	G3 (eV)
#1	–	–	–
#2	235.6	232.2	–
#3	235.9	232.5	230.0
#4	235.5	232.7	230.4
#5	235.3	232.9	230.4
[a] Mo^{6+} $3d_{3/2}$	235.8		
[a] Mo^{6+} $3d_{5/2}$		232.6	
[b] Mo^{4+} $3d_{3/2}$		233.2	
[b] Mo^{4+} $3d_{5/2}$			230.1

[a] Ref. [12].
[b] Ref. [13].

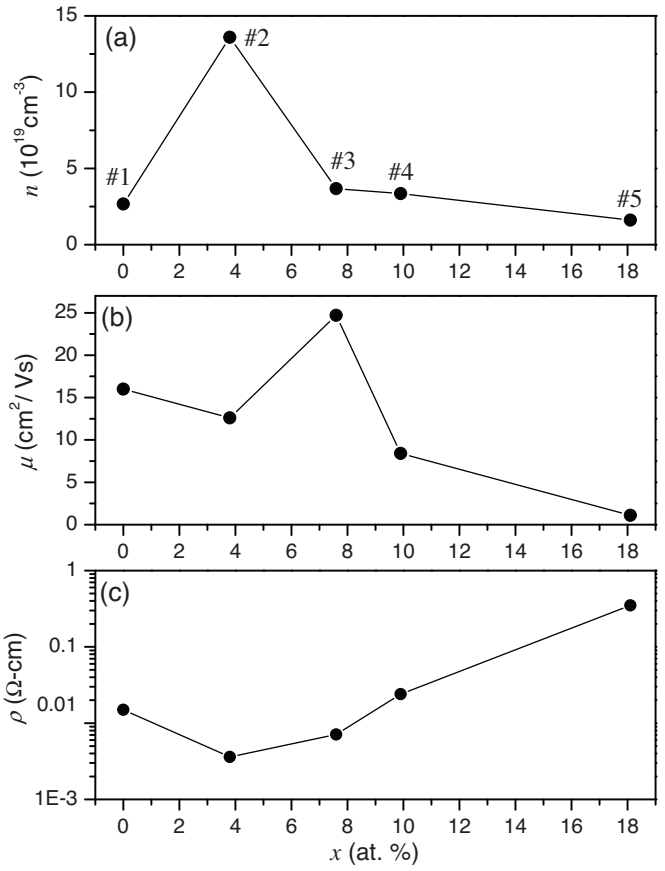

Fig. 3. Electrical properties including (a) carrier density n, (b) carrier mobility μ and (c) resistivity ρ of x at.% Mo-doped a-IGZO films. x at.% = [Mn]/[In].

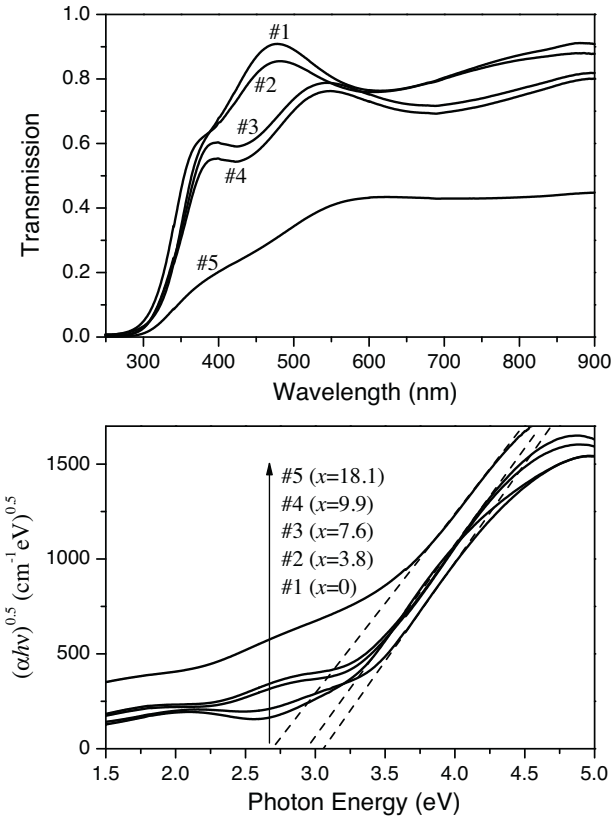

Fig. 4. (a) Transmission spectra and (b) $(\alpha h\nu)^{0.5}$ vs $h\nu$ plots for x at.% Mo-doped a-IGZO films.

ratio [Mo]/[In] of Mo-doped a-IGZO film. As shown in Fig. 3(a), the carrier density (n) of sample #2 is about 13.6×10^{19} cm^{-3}, which is much higher than that of the undoped film whose value of n is 2.7×10^{19} cm^{-3}. The increase of carrier density can be attributed to the extra electrons provided by Mo^{6+} doped in a-IGZO films. On the other hand, carrier densities of samples #3, #4 and #5 are 3.7×10^{19}, 3.4×10^{19} and 1.7×10^{19} cm^{-3}, respectively, which decrease with increasing the Mo doping. The carrier mobilities of films are shown in Fig. 4(b). It is noteworthy that, in comparison with the undoped film (sample #1), the carrier mobility of sample #3 is distinctly enhanced. The enhancement of the carrier mobility similar to that observed in Mo-doped In_2O_3 films [9,10] can be explained by the magnetic interactions resulting in smaller effective mass of carriers and larger fundamental bandgap [11]. Except for the sample #3, the carrier mobility decreases with the Mo doping. It can be attributed to the increase of the density of Mo ions which serve as strong scattering centers and thus suppress the transport of charge carriers. The low carrier mobility of sample #2, compared to that of sample #3, is attributed to the free-carrier scattering, since the carrier density of sample #2 is much higher than that of other samples. The electrical experiments reveal that the carrier density and mobility of a-IGZO films can be enhanced by Mo doping with a proper concentration. On the other hand, the resistivities of low concentration Mo-doped films (samples #2 and #3) are lower than that of the undoped film (sample #1) but increase with increasing Mo concentration, as shown in Fig. 3(c), which is resulted from the decrease of carrier mobility with increasing the Mo concentration (except for the sample #3).

The transmission spectra of all films are illustrated in Fig. 4(a). The transmission of the undoped film (sample #1) exceed 80% in the visible range (400–700 nm); however, the transmission decreases with increasing the Mo doping. Moreover, the absorption edge of sample #2, the a-IGZO film doped with 3.8 at.% Mo, shifts toward shorter wavelength region. The optical band gaps (E_g) of these films can be estimated by the relationship between absorption coefficient (α) and photon energy ($h\nu$) of the form $(\alpha h\nu) \sim (h\nu - E_g)^r$ with $r = 2$ suggested by Tauc for amorphous semiconductors [14,15]. The E_g of samples #1, #3 and #4 is about 2.95 eV obtained by linear extrapolation of $(\alpha h\nu)^{0.5}$ to the $h\nu$-axis, as depicted in Fig. 4(b). The E_g of sample #2 is about 3.05 eV which is slightly higher than that of the undoped sample #1 and can be attributed to the Burstein–Moss (BM) effect, since the carrier density of sample #2 is much higher than that of the sample #1. The same E_g of samples #1, #3 and #4 and BM effect observed for sample #2 imply the incorporation of Mo atoms in the IGZO lattices. On the other hand, the E_g of sample #5 is 2.7 eV which is believed to be resulted from the high concentration of Mo doping which may result in the possible existence of Mo oxide impurities.

Fig. 5 shows the field dependence of magnetization $M(H)$ curves measured at 300 K for the undoped and Mo-doped a-IGZO films. The undoped film (sample #1) shows a linear $M(H)$ curve which indicates paramagnetic behavior. All Mo-doped films obviously exhibit room-temperature ferromagnetism. Moreover, except the sample #3, the magnetization increases with increasing the Mo doping. According to Medvedeva's study, the exchange splitting of d states results in the magnetic moments of Mo atoms [11]. However, Medvedeva's calculations suggest a very weak magnetic coupling between Mo dopants and ferromagnetism which would not be observed in Mo-doped In_2O_3. It is not consistent with our experimental results and similar ferromagnetism in Mo-doped In_2O_3 films was also observed [16]. The ferromagnetism observed in this work could be attributed to the free-electron mediated ferromagnetic interaction [17,18] between the magnetic Mo ions.

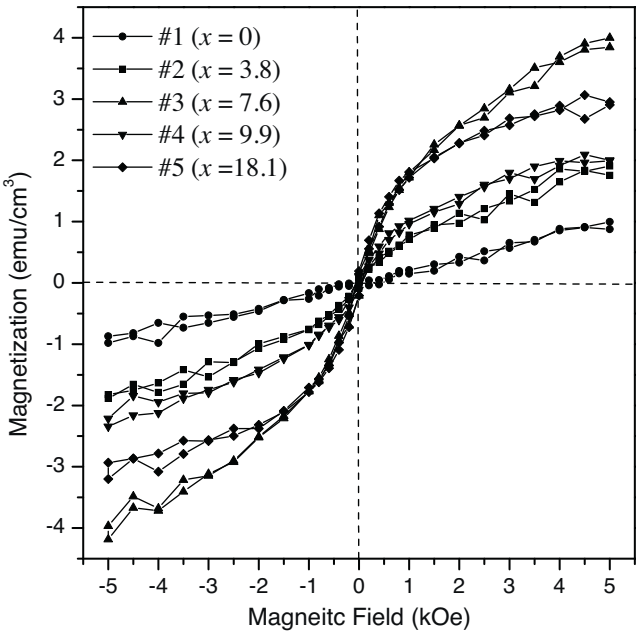

Fig. 5. Field (H) dependent magnetization (M) of x at.% Mo-doped a-IGZO films measured at room temperature.

The correlation between the high magnetization and high mobility observed for sample #3 supports the free-electron mediated model.

4. Conclusions

In conclusion, the valence of Mo ions is 6+ in low concentration Mo doped a-IGZO films and becomes a mixture of 6+ and 4+ with increasing the Mo doping level. The carrier mobility and carrier density of a-IGZO films can be enhanced by Mo doping with a proper concentration. The optical transmission of a-IGZO films is decreased by the Mo doping. Nevertheless, the optical bandgap is not significantly affected by the Mo doping. However, a blue shift in transmission spectra resulted from Burstein–Moss effect was observed in low-concentration Mo doping. Furthermore, all Mo-doped films exhibit room-temperature ferromagnetism. The carrier mobility of the Mo-doped sample exhibiting the largest magnetization is remarkably enhanced by Mo doping. The result reveals the correlation between the enhancement of the carrier mobility and ferromagnetic characteristics.

Acknowledgment

This work was supported by the National Science Council of Taiwan, under Grant No. NSC 98-2112-M-003-005-MY3.

References

[1] Nomura, K. Ohta, H. Takagi, A. Hirano, M. Hosono,H. Nature 432 (2004) 488.
[2] Chiang, H.Q. Wager, J.F. Hoffman, R.L. Jeong, J. Keszler,D.A. Appl. Phys. Lett. 86 (2005) 013503.
[3] Lee, J.H. Kim, D.H. Yang, D.J. Hong, S.Y. Yoon, K.S. Hong, P.S. Jeong, C.O. Park, H.S. Kim, S.Y. Lim, S.K. Kim, S.S. Son, K.S. Kim, T.S. Kwon, J.Y. Lee,S.Y. SID Int. Symp. Digest Tech. Pap. 39 (2008) 625.
[4] Orita, M. Tanji, H. Mizuno, M. Adachi, H. Tanaka,I. Phys. Rev. B 61 (2000) 1811.
[5] Takagi, A. Nomura, K. Ohta, H. Yanagi, H. Kamiya, T. Hirano, M. Hosono,H. Thin Solid Films 486 (2005) 38.
[6] Nomura, K. Kamiya, T. Ohta, H. Shimizu, K. Hirano, M. Hosono,H. Phys. Status Solidi A 205 (2008) 1910.
[7] Liu, S.J. Fang, H.W. Su, S.H. Li, C.H. Cherng, J.S. Hsieh, J.H. Juang,J.Y. Appl. Phys. Lett. 94 (2009) 092504.
[8] Liu, S.J. Su, S.H. Fang, H.W. Hsieh, J.H. Juang,J.Y. Appl. Surf. Sci. 157 (2011) 10018.
[9] Sun, S.Y. Huang, J.L. Lii,D.F. J. Mater. Res. 20 (2005) 247.
[10] Gupta, R.K. Ghosha, K. Mishrab, S.R. Kahol,P.K. Appl. Surf. Sci. 254 (2008) 4018.
[11] Medvedeva,J.E. Phys. Rev. Lett. 97 (2006) 086401.
[12] Wagner, C.D. Riggs, W.M. Davis, L.E. Moulder, J.F. Muilenberg,G.E. Handbook of X-ray Photoelectron Spectroscopy, Perkin-Elmer, Eden Prairie, MN, 1979.
[13] Choi, J.G. Thompson,L.T. Appl. Surf. Sci. 93 (1996) 143.
[14] Tauc,J. Amorphous and Liquid Semiconductors, Plenum, New York, 1979.
[15] Jayaraj, M.K. Saji, K.J. Normura, K. Kamiya, T. Hosono,H. J. Vac. Sci. Technol. B 26 (2008) 495.
[16] Park, C.Y. Yoon, S.G. Jo, Y.H. Shin,S.C. Appl. Phys. Lett. 95 (2009) 122502.
[17] Dietl, T. Ohno, H. Matsukura, F. Cibert, J. Ferrand,D. Science 287 (2000) 1019.
[18] Sato, K. Yoshida,H.K. Jpn. J. Appl. Phys., Part 2 39 (2000) L555.